THE JOURNAL OF PHYSICAL CHEMISTRY Letters

Letter

pubs.acs.org/JPCL

Thermodynamics of Helix−Coil Transitions of Polyalanine in Open Carbon Nanotubes

Dylan Suvlu,*[,†] Seneviratne Samaratunga,[†] D. Thirumalai,[‡] and Jayendran C. Rasaiah*[,†]

[†]Department of Chemistry, University of Maine, Orono, Maine 04469, United States

[‡]Department of Chemistry, The University of Texas at Austin, Austin, Texas 78712, United States

Supporting Information

ABSTRACT: Understanding structure formation in polypeptide chains and synthetic polymers encapsulated in pores is important in biology and nanotechnology. We present replica exchange molecular dynamics studies of the phase diagram for α-helix formation of capped polyalanine in nanotubes (NT) open to a water reservoir as a function of the NT diameter and hydrophobicity. A helix forms only in a narrow range of diameters, which surprisingly is comparable to the width of the ribosome tunnel. Increasing the hydrophobicity enhances helicity in the NT. Helix formation in polyalanine is driven by a small negative enthalpy and a positive entropy change at ≈300 K, in contrast to the large negative entropy change that destabilizes the helix and favors the coiled state in bulk water. There is an anticorrelation between water density inside the nanotube and structure formation. Confinement-induced helix formation depends on amino acid sequence. There is complete absence of helix in polyglutamine and polyserine confined to a open carbon nanotube.

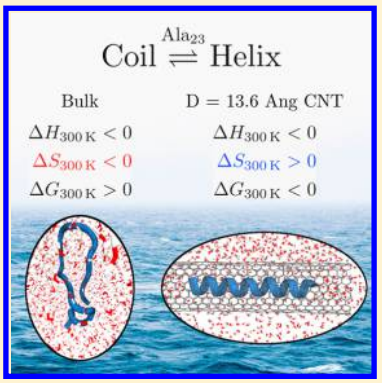

Confinement of biopolymers and synthetic materials in nanopores play an important role in DNA sequencing,[1] drug delivery,[2] biotechnology applications,[3] folding,[4,5] degradation of proteins,[6] and in the design of biosensors.[7,8] The structural transitions that occur when water-soluble synthetic polymers are encapsulated in nanotubes (NT) are important in the design of nanomaterials for use in membrane separation and energy related applications. Another example of considerable interest in biology is the influence of the cylindrical ribosome tunnel through which the newly synthesized protein must pass and how it facilitates structure formation.[9−13] The tunnel diameter varies between 10 and 20 Å with an average of approximately 15 Å.[14] A number of experiments have shown there are zones within the tunnel that are conducive to compaction and α-helix formation.[9−13,15] Theoretical studies indicate conformational restrictions of the coiled state in a confined system make it entropically more unfavorable than the α-helix, thus favoring the formation of the helical state.[16−18] We investigate this here and study the thermodynamics of coil−helix transition of polyalanine encapsulated in nanotubes open to water reservoirs.

We present results of an all-atom replica exchange molecular dynamics (MD) study of helix formation in capped 23-alanine ($COCH_3$-A_{23}-$NHCH_3$) confined to NTs. The NTs are open to a water reservoir implying that, at equilibrium, the chemical potentials of the bulk and confined water are identical. Using extensive converged atomically detailed simulations covering a broad range of temperature and differing values of the NT diameter (D), we discovered the following key results. (1) We find that the 23 alanine peptide (A_{23}) forms a stable helix over a narrow optimal range of D (≈ 13−15 Å). The helix content, which changes nonmonotonically with D, decreases precipitously outside the optimal range of D. (2) By varying the hydrophobicity of the confining carbon nanotube we demonstrate that there is an anticorrelation between the extent of hydration and the α-helical content. In other words, in the optimal range of D, A_{23} adopts a helical structure in the region of carbon NT, which is essentially devoid of water. (3) Interestingly, thermodynamic analyses show that the observed transition from coil to helix in A_{23} is driven by a negative enthalpy change in the temperature range 280−500 K and a small positive change in entropy below ≈350 K due to nanoconfinement. This is dramatically different from the behavior in bulk water in which a large unfavorable (negative) entropy change for the coil to helix transition overwhelms the accompanying negative enthalpy change, except below ≈290 K for the CHARMM36 force field. All of the results are qualitatively insensitive to the force fields employed, but there are quantitative differences.

In order to establish the robustness of our results, we used three different force fields (AMBER99SB*-ILDN,[19,20] CHARMM36,[21,22] and CHARMM22[23,24]). The CHARMM22 force field has a strong propensity to form α-helices in polypeptides.[19,21] We confirmed this in our replica exchange simulations of A_{23} in bulk water and NTs (see Supporting Information (SI)) and discarded it in favor of the AMBER99SB* and CHARMM36 force fields. To model the changes in the tunnel-peptide interactions, we scaled the Lennard-Jones interaction of the carbon atoms in the NT using a parameter λ,

Received: November 8, 2016
Accepted: January 6, 2017
Published: January 6, 2017

DOI: 10.1021/acs.jpclett.6b02620
J. Phys. Chem. Lett. 2017, 8, 494−499

Table 1. Thermodynamic Fits to the Data Using the Expression $\ln K(T) = -(n-2)\Delta H_{300K}/RT - (n-2)\Delta C_P(1 - 300\ \mathrm{K}/T)/R + n\Delta S_{300K}/R + n\Delta C_P \ln [T/300\mathrm{K}])/R$[30,31]

force field	λ	$\Delta H_{300\ K}$ kJ mol^{-1} res^{-1}	$\Delta S_{300\ K}$ J mol^{-1} K^{-1} res^{-1}	ΔC_P J mol^{-1} K^{-1} res^{-1}
		bulk		
charmm36		−1.37 (0.02)	−4.24 (0.06)	+3.25 (0.18)
amber99sb*		−0.54 (0.02)	−2.30 (0.06)	+2.08 (0.16)
		D = 13.6 Å		
charmm36	1.0	−0.31 (0.01)	+0.41 (0.01)	−2.05 (0.04)
charmm36	0.80	−0.39 (0.01)	+0.23 (0.02)	−1.85 (0.05)
charmm36	0.64	−0.46 (0.01)	+0.07 (0.02)	−1.71 (0.04)
charmm36	0.56	−0.47 (0.01)	+0.05 (0.02)	−1.67 (0.05)
amber99sb*	1.0	−0.08 (0.00)	+0.63 (0.01)	−2.38 (0.03)
amber99sb*	0.80	−0.14 (0.00)	+0.50 (0.01)	−2.16 (0.04)
amber99sb*	0.64	−0.18 (0.00)	+0.40 (0.01)	−2.11 (0.04)
amber99sb*	0.56	−0.20 (0.00)	+0.36 (0.01)	−2.06 (0.03)

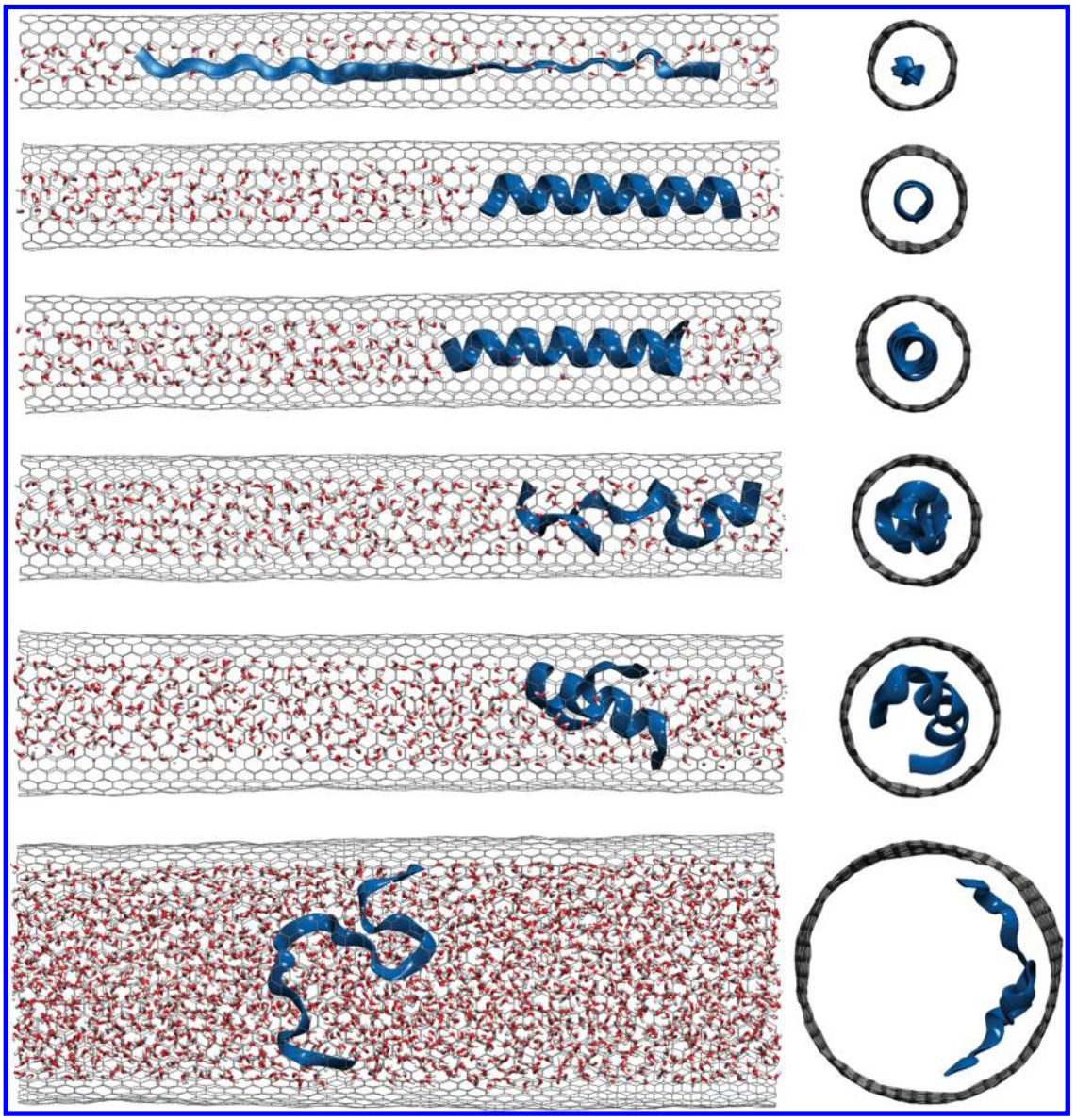

Figure 1. Randomly selected equilibrium conformations of A_{23} in NTs with diameter (from top) D = 12.2, 13.6, 14.9, 16.3, 20.4, and 35.3 Å for λ = 1.0 at 300 K obtained using the CHARMM36 force field. Images from the AMBER force field are in the SI.

which can take on values from zero to unity.[17] For the values used in our simulations, λ = 1.0, 0.80, 0.64 and 0.56, A_{23} is stably encapsulated in the NT.

We performed replica exchange molecular dynamics simulations using GROMACS 5.1.2[25] for A_{23} in bulk water and in armchair (n,n) NTs with lengths of 100 Å and diameters (D =

DOI: 10.1021/acs.jpclett.6b02620
J. Phys. Chem. Lett. 2017, 8, 494−499

0.783 Å$\sqrt{3n}$) of 12.2, 13.6, 14.9, 16.3, and 20.4 Å. The NTs were immersed in a water bath with hexagonal periodic boundary conditions. The 12.2, 13.6, and 14.9 Å NT systems each contained 74 replicas, while the 16.3 and 20.4 Å systems each contained 84 and 88 replicas, respectively. The convergence time of each system varied, and we monitored the results for convergence by analyzing the structure of A_{23} with time. A table of simulation length per replica is provided in the SI. Simulated annealing was conducted for the largest NT (D = 35.3 Å) with a simulation length of 200 ns. The temperature range of the replicas was 280−500 K, where the temperature spacing was determined by following the procedure described elsewhere[26] such that the exchange probability was at least 0.23 (±0.02) with replica exchange attempts every 1 ps. This also generates the data necessary to compute the thermodynamics of helix formation (Table 1). Our replica exchange calculations were validated by comparing our results for the thermodynamics of helix−coil transition in TIP3P water with previous studies[19,21] with good agreement. Errors are estimated by block averaging.[27] Additional details of the systems and the simulations are in the SI.

Snapshots of the equilibrated polypeptide for the CHARMM36 force field in each NT (Figure 1) give a picture of the opposing influence of confinement and hydration. The most important observation is that, for all D, a helix forms along the axis of the tube only in regions depleted of water molecules and over a narrow range of diameters. The fractional helix content Θ_H (see SI for details) as a function of tube diameter for λ = 1.0 (least hydrophobic) is displayed in Figure 2. The striking

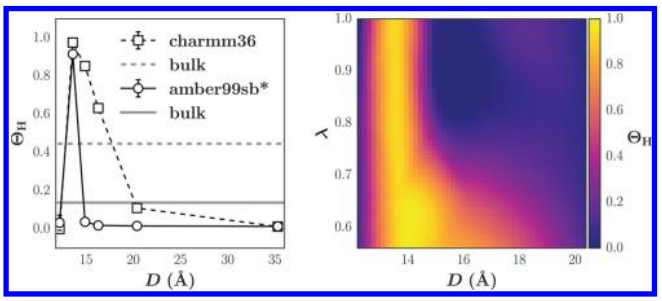

Figure 2. (Left) Fractional helix content Θ_H of A_{23} encapsulated in a NT of varying diameters with λ = 1.0 at 300 K for CHARMM36 and AMBER99SB*-ILDN force fields. Horizontal lines are the values of Θ_H in bulk water. Where error bars are not visible, they are smaller than the symbol. (Right) Phase diagram of Θ_H at 300 K in the (D, λ) plane for the AMBER99SB*-ILDN force field shows that for all λ, helix formation occurs only over a limited range of D values.

aspect of the results in Figure 2 is that Θ_H changes nonmonotonically with D. There is complete absence of helix content for large D with Θ_H being even less than in bulk water for the CHARMM36 and AMBER99SB* force fields. Helices form only when the diameter of the nanotube is larger than 12.2 Å and smaller than 20.4 Å, with the optimal diameter for the pristine α-helix being close to 13.6 Å. Interestingly, this value is comparable to the average diameter ($D \approx 15$ Å) of the region in the ribosome tunnel where α-helix formation is most favorable.[13,15] As D decreases below 13.6 Å, Θ_H decreases precipitously, which tidily explains the absence of compaction of polypeptide chains in the region of constriction located in lower part of the ribosome tunnel. For D = 12.2 Å, A_{23} is extended with $\Theta_H \approx 0$. Similarly, Θ_H is greatly reduced in the NTs with $D \geq$ 20.4 Å, when the polypeptide is adsorbed onto the interior wall of the NT. The prediction that A_{23} forms an α-helix is in contrast with a previous study,[28] which showed that helix formation does not occur in the physically unrealistic periodically replicated NT that precludes flow of water in or out to maintain chemical equilibrium with an external reservoir. Figure 4 illustrates that the (ϕ, ψ) angles are localized predominantly in the α-helical region.[29]

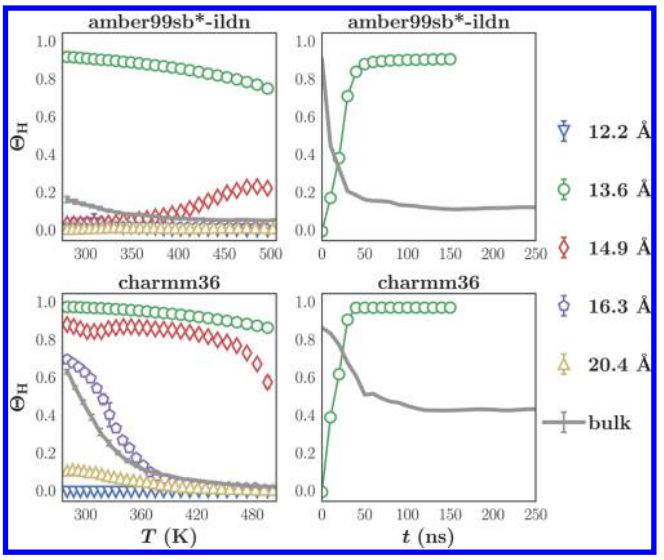

Figure 3. Fractional helix content Θ_H as a function of T (K) (for λ = 1.0) and t (ns) (at 300 K) of A_{23} in the NTs and bulk water. In the plots of Θ_H versus T, only every third data point is plotted for clarity. Where error bars are not visible they are smaller than the symbol.

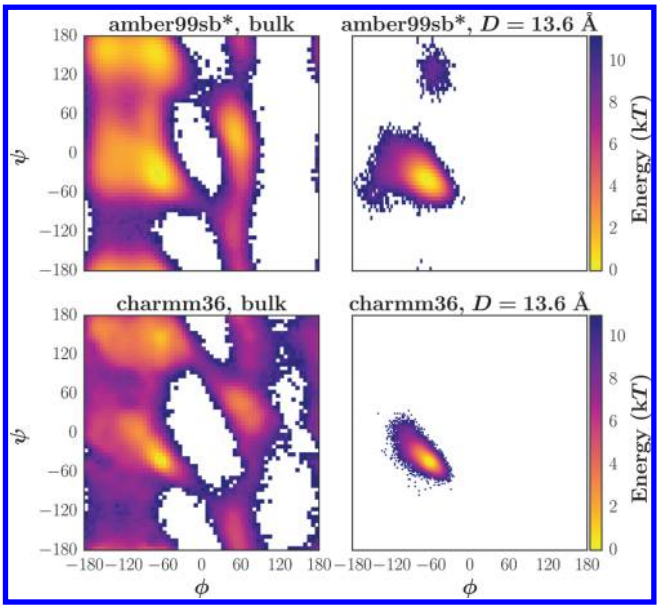

Figure 4. Ramachandran potentials of mean force −ln $P(\phi,\psi)$ of the inner 21 residues in A_{23} in D = 13.6 Å NTs and bulk water for both force fields at 300 K.

Figure 2 shows a phase diagram for helix formation in which Θ_H is plotted as a function of D and λ. It is clear that, for D = 13.6 Å, Θ_H achieves a maximum for all $\lambda \geq$ 0.56. Changes in D and λ have significant effects on the stability of the α-helix. Small changes in λ broaden the optimal D for which Θ_H is a maximum. As λ decreases from 1.0 through 0.80 and 0.64 to 0.56, the NT becomes more hydrophobic (see Table 2), resulting in an increase in Θ_H for $D \geq$ 13.6 Å. Additionally, the phase diagram in

DOI: 10.1021/acs.jpclett.6b02620
J. Phys. Chem. Lett. 2017, 8, 494−499

Table 2. Fractional Helicity Θ_H, Number of Water Molecules Inside the NT N_W, and Number of Peptide−Peptide N_{PP} and Peptide−Water N_{PW} Hydrogen Bonds at 300 K for Each λ

force field	λ	Θ_H	N_W	N_{PP}	N_{PW}
		D = 13.6 Å			
amber99sb*	1.0	0.9509 ± 0.0006	151	20.35	8.14
amber99sb*	0.80	0.9561 ± 0.0007	144	20.47	7.69
amber99sb*	0.64	0.9598 ± 0.0006	137	20.56	7.35
amber99sb*	0.56	0.9614 ± 0.0004	133	20.59	7.15
		D = 14.9 Å			
amber99sb*	1.0	0.037 ± 0.002	225	3.50	29.17
amber99sb*	0.80	0.201 ± 0.021	212	6.29	25.85
amber99sb*	0.64	0.905 ± 0.005	187	18.41	7.02
amber99sb*	0.56	0.923 ± 0.002	182	18.66	6.50

the (D, T) plane displayed in the SI for both force fields shows that the helix is stable up to a temperature of ∼500 K in the D = 13.6 Å NT.

The thermodynamics of helix formation in A_{23} are determined by fitting $\Delta G_{HC} = -RT \ln K(T) = \Delta H_{total}(T) - T\Delta S_{total}(T) = (n-2)\,\Delta H_{res}(T) - nT\Delta S_{res}(T)$[30,31] (see SI for details) to the data where $K = \Theta_H/(1-\Theta_H)$ and n = 23 is the number of residues (Figure 5 and Table 1). The enthalpy, entropy, and heat capacity change of helix formation in A_{23} in bulk water are qualitatively consistent with previous estimates from experiment[32] and simulation.[33] The enthalpy and entropy of helix formation is greater in magnitude for the CHARMM36 force field in bulk water than for the AMBER99SB* force field (Table 1 and Figure 5), as found previously.[21] However, the all-or-nothing two-state helix−coil model used to obtain the thermodynamic values in Table 1 underestimate both the enthalpy and entropy of helix formation in the bulk phase. Experiment shows the enthalpy of helix formation in alanine-based polypeptides to be ≈ −3.8 kJ mol^{-1} res^{-1},[32] but bulk water simulations with the CHARMM36 force field give a value of ≈ − 1.4 kJ mol^{-1} res^{-1}. To account for the imperfect cooperative nature of the helix−coil transition, we fit our data to the Lifson−Roig model (see SI) which gives a value of −3.29 kJ mol^{-1} res^{-1} for the enthalpy of helix formation with the CHARMM36 force field in bulk water.

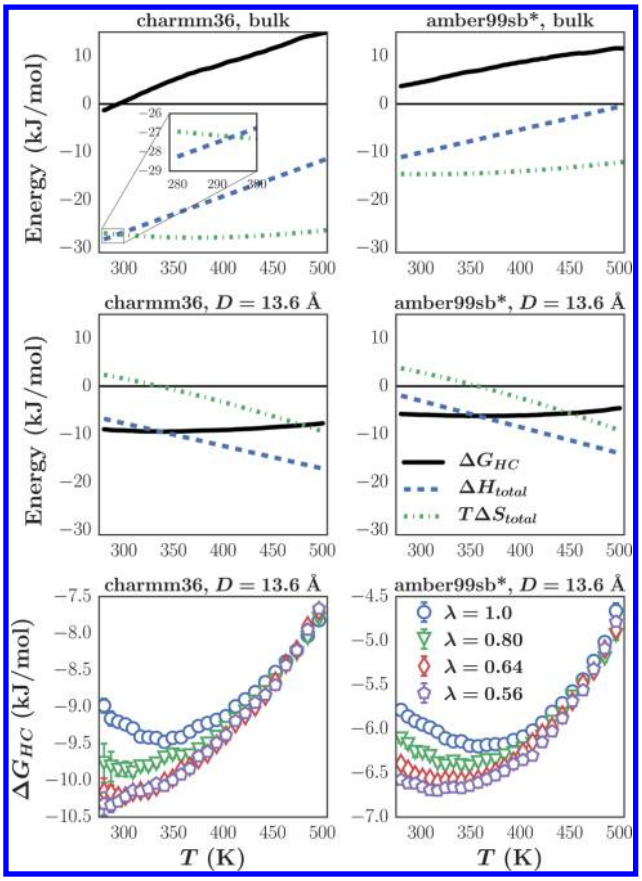

Figure 5. Top four panels display the Gibbs free energy $\Delta G_{HC} = -RT \ln K(T)$ (solid line), enthalpy ΔH_{total} (dashed line), and entropy $T\Delta S_{total}$ (dashed-dotted line) of helix formation for bulk water and the D = 13.6 Å NT for both force fields with λ = 1.0. The bottom two panels display the Gibbs free energy for different λ for both force fields in the D = 13.6 Å NT.

Figure 5 shows that helix formation in A_{23} in bulk water is unfavorable except below ≈290 K with the CHARMM36 force field, but is favorable in the D = 13.6 Å NT even up to 500 K. Inside the D = 13.6 Å, NT helix formation at 300 K is driven by a negative ΔH and a positive ΔS (Table 1 and Figure 5). However, the enthalpy change in the D = 13.6 Å is less negative than in bulk water. Importantly, ΔC_p in the D = 13.6 Å NT is negative, the opposite of ΔC_p in bulk water, which completely alters the temperature dependence of ΔH_{total} and ΔS_{total} in the D = 13.6 Å NT. As the temperature increases, both ΔH_{total} and $T\Delta S_{total}$ decrease, but $T\Delta S_{total}$ decreases at a greater rate resulting in a slight increase in ΔG_{HC} with temperature (Figure 5). Table 1 shows how ΔH_{300K} and ΔS_{300K} vary with λ. As λ decreases from 1.0 to 0.56, ΔH_{300K} becomes more negative and ΔS_{300K} becomes less positive. The net result is the helix becomes more stable as λ decreases as displayed in Figure 5. Furthermore, the free energy displays a minimum inside the D = 13.6 Å NT, which shifts to lower temperatures as λ decreases (Figure 5). Based on polymer physics of confinement, it was argued that the positive difference between ΔS_{NT} and ΔS_{bulk} could stabilize the helix state over a narrow range of tube diameters.[16] Although this trend is borne out from our simulations, we also note that enthalpy is a major driving force for helix formation inside the D = 13.6 Å NT. Furthermore, the release of hydrating water molecules from the peptide during this process contributes to the positive change in entropy observed in our simulations.

We now elaborate on the role of water molecules in helix formation of A_{23} as a function of D to illustrate the interplay between confinement and hydration effects. A helical polypeptide occupies more space (larger excluded volume) in the NT than conformations lacking structure. The larger excluded volume of the ordered state leads to release of water molecules from the vicinity of the ordered α-helix, explaining the anticorrelation between hydration and structure formation. This is vividly illustrated in Table 2 and Figure 1. The number of water molecules in the NT and the number of hydrogen bonded waters to A_{23} decrease with decreasing λ (Table 2). When D = 13.6 Å and λ = 0.56, Θ_H is a maximum and N_W is a minimum. A similar, more pronounced trend occurs in the D = 14.9 Å NT. These results show quantitatively that helix formation is anticorrelated with the removal of water molecules from the vicinity of the polypeptide and its expulsion from the NTs into a reservoir. A corollary of this finding is if the peptide were hydrated in the NT, the helical state of A_{23} would be destabilized. In this case, the extended state would be stabilized by favorable peptide−NT interactions and interactions between the peptide and water (Figure 1 for illustrations). In contrast to the absence of water in the vicinity of the helix, a recent study[34] found that in narrow pores, the water-soluble poly(ethylene oxide) is hydrated

DOI: 10.1021/acs.jpclett.6b02620
J. Phys. Chem. Lett. 2017, 8, 494−499

in carbon nanotubes, indicating hydration effects on encapsulated peptides and polymers depend on the sequence. Furthermore, our replica exchange simulations show no helix formation in polyglutamine and polyserine in nanotubes with diameters of 16.3 and 13.6 Å respectiveley.

Based on replica exchange molecular dynamics simulations of polyalanine (A_{23}) in NTs open to a water reservoir over a range of diameters (D = 12.2−35.3 Å) and temperatures (T = 280−500 K, Figure 3), we find that confinement and hydration promote helix formation only over a narrow range of D. In contrast to the bulk, A_{23} forms thermodynamically stable α-helices upon encapsulation in open NTs within a narrow range of diameters from ≈13−15 Å, which is remarkably close to the average diameter of the ribosome tunnel.[13] Interestingly, water is expelled from the vicinity of the ordered state of A_{23} (Figure 1) implying that helix formation is anticorrelated with the number of water molecules inside the NT (Table 2). Increase in the hydrophobicity of the tubes broadens the range of diameters for optimal helix formation as displayed in a phase diagram in the (D, λ) plane (Figure 2). The thermodynamics of helix formation obtained from the temperature dependence of the fractional helical content Θ_H of A_{23} with D = 13.6 Å shows that α-helix formation is driven by favorable negative enthalpy and positive entropy change from the coiled to helical state at 300 K. By contrast, the large negative entropy change for this process in bulk water inhibits helix formation. To our knowledge, this is the first report on the thermodynamics and the existence of a critical range of diameters for helix formation in a polypeptide chain confined to nanotubes in the presence of molecular water. Given that the subtle interplay between enthalpy, entropy, and hydration determines α-helix formation, it follows that the extent of structure formation in nanotubes and in the tunnel of the ribosome should depend on the precise polypeptide sequence. Thus, based on our findings, which are qualitatively robust to changes in force fields, we surmise that atomically detailed simulations of an open system are needed to decipher the mechanism of helix formation in nanopores and the biologically relevant ribosome tunnel.

■ ASSOCIATED CONTENT

Supporting Information

The Supporting Information is available free of charge on the ACS Publications website at DOI: 10.1021/acs.jpclett.6b02620.

Additional details of the simulation and analysis methods; images of A_{23} inside the NT for the CHARMM22 and AMBER99SB*-ILDN force fields; simulation length for each system; phase diagrams in the (D, T) plane; fractional helicity for the CHARMM22 force field; Lifson−Roig (LR) parameters extracted from the simulations using a Bayesian formalism; thermodynamic fits to the LR parameters (PDF)

■ AUTHOR INFORMATION

Corresponding Authors

*E-mail: dylan.suvlu@maine.edu.
*E-mail: rasaiah@maine.edu.

ORCID

D. Thirumalai: 0000-0003-1801-5924
Jayendran C. Rasaiah: 0000-0002-4453-7438

Notes

The authors declare no competing financial interest.

■ ACKNOWLEDGMENTS

We thank S. Vaitheeswaran for advice. The technical assistance of Eric Lovejoy is gratefully acknowledged. We especially thank Stephen Cousins of the University of Maine Advanced Computing Group for his support and for significant allotments of computation time. J.C.R. and D.T. thank the National Science Foundation for grant support.

■ REFERENCES

(1) Kasianowicz, J. J.; Brandin, E.; Branton, D.; Deamer, D. W. Characterization of Individual Polynucleotide Molecules Using a Membrane Channel. *Proc. Natl. Acad. Sci. U. S. A.* **1996**, *93*, 13770−13773.

(2) Battigelli, A.; Russier, J.; Venturelli, E.; Fabbro, C.; Petronilli, V.; Bernardi, P.; Da Ros, T.; Prato, M.; Bianco, A. Peptide-Based Carbon Nanotubes for Mitochondrial Targeting. *Nanoscale* **2013**, *5*, 9110−9117.

(3) Bekyarova, E.; Ni, Y.; Malarkey, E. B.; Montana, V.; McWilliams, J. L.; Haddon, R. C.; Parpura, V. Applications of Carbon Nanotubes in Biotechnology and Biomedicine. *J. Biomed. Nanotechnol.* **2005**, *1*, 3−17.

(4) Gumbart, J.; Chipot, C.; Schulten, K. Free Energy of Nascent-Chain Folding in the Translocon. *J. Am. Chem. Soc.* **2011**, *133*, 7602−7607.

(5) Thirumalai, D.; Lorimer, G. H. Chaperonin-Mediated Protein Folding. *Annu. Rev. Biophys. Biomol. Struct.* **2001**, *30*, 245−269.

(6) Stinson, B. M.; Nager, A. R.; Glynn, S. E.; Schmitz, K. R.; Baker, T. A.; Sauer, R. T. Nucleotide Binding and Conformation Switching in the Hexametric Ring of AAA+ Machine. *Cell* **2013**, *153*, 628−639.

(7) Tu, Y.; Zhou, R.; Fang, H. Signal Transmission, Conversion and Multiplication by Polar Molecules Confined in Nanochannels. *Nanoscale* **2010**, *2*, 1976−1983.

(8) Tu, Y.; Xiu, P.; Wan, R.; Hu, J.; Zhou, R.; Fang, H. Water-Mediated Signal Multiplication with Y-Shaped Carbon Nanotubes. *Proc. Natl. Acad. Sci. U. S. A.* **2009**, *106*, 18120−18124.

(9) Yonath, A. Hibernating Bears, Antibiotics, and the Evolving Ribosome. *Angew. Chem., Int. Ed.* **2010**, *49*, 4340−4354.

(10) Ramakrishnan, V. Unraveling the Structure of the Ribosome. *Angew. Chem., Int. Ed.* **2010**, *49*, 4355−4380.

(11) Tu, L. W.; Deutsch, C. A Folding Alone in the Ribosomal Exit Runnel for Kv1.3 Helix Formation. *J. Mol. Biol.* **2010**, *396*, 1346−1360.

(12) Bhushan, S.; Gartmann, M.; Halic, M.; Armache, J.-P.; Jarasch, A.; Mielke, T.; Berninghausen, O.; Wilson, D. N.; Beckmann, R. α-Helical Nascent Polypeptide Chains Visualized Within Distinct Regions of the Ribosomal Exit Tunnel. *Nat. Struct. Mol. Biol.* **2010**, *17*, 313−317.

(13) Wilson, D. N.; Beckmann, R. The Ribosomal Tunnel as a Functional Environment for Nascent Polypeptide Folding and Translational Stalling. *Curr. Opin. Struct. Biol.* **2011**, *21*, 274−282.

(14) Bogdanov, A. A.; Sumbatyan, N. V.; Shishkina, A. V.; Karpenko, V. V.; Korshunova, G. A. Ribosomal Tunnel and Translation Regulation. *Biochemistry* **2010**, *75*, 1501−1516.

(15) Woolhead, C. A.; McCormick, P. J.; Johnson, A. E. Nascent Membrane and Secretory Proteins Differ in FRET-Detected Folding Far Inside the Ribosome and in Their Exposure to Ribosomal Proteins. *Cell* **2004**, *116*, 725−736.

(16) Ziv, G.; Haran, G.; Thirumalai, D. Ribosome Exit Tunnel can Entropically Stabilize α-Helices. *Proc. Natl. Acad. Sci. U. S. A.* **2005**, *102*, 18956−18961.

(17) O'Brien, E. P.; Stan, G.; Thirumalai, D.; Brooks, B. R. Factors Governing Helix Formation in Peptides Confined to Carbon Nanotubes. *Nano Lett.* **2008**, *8*, 3702−3708.

(18) Vaitheeswaran, S.; Thirumalai, D. Interactions Between Amino Acid Side Chains in Cylindrical Hydrophobic Nanopores with Applications to Peptide Stability. *Proc. Natl. Acad. Sci. U. S. A.* **2008**, *105*, 17636−17641.

(19) Best, R. B.; Hummer, G. Optimized Molecular Dynamics Force Fields Applied to the Helix-Coil Transition of Polypeptides. *J. Phys. Chem. B* **2009**, *113*, 9004−9015.

DOI: 10.1021/acs.jpclett.6b02620
J. Phys. Chem. Lett. 2017, 8, 494−499

(20) Lindorff-Larsen, K.; Maragakis, P.; Piana, S.; Eastwood, M. P.; Dror, R. O.; Shaw, D. E. Systematic Validation of Protein Force Fields Against Experimental Data. *PLoS One* **2012**, *7*, e32131.
(21) Best, R. B.; Mittal, J.; Feig, M.; MacKerell, A. D. Inclusion of Many-Body Effects in the Additive CHARMM Protein CMAP Potential Results in Enhanced Cooperativity of α-Helix and β-Hairpin Formation. *Biophys. J.* **2012**, *103*, 1045−1051.
(22) Best, R. B.; Zhu, X.; Shim, J.; Lopes, P. E.; Mittal, J.; Feig, M.; MacKerell, A. D., Jr Optimization of the Additive CHARMM All-Atom Protein Force Field Targeting Improved Sampling of the Backbone ϕ, ψ and Side-Chain χ1 and χ2 Dihedral Angles. *J. Chem. Theory Comput.* **2012**, *8*, 3257−3273.
(23) MacKerell, A. D.; Bashford, D.; Bellott, M.; Dunbrack, R. L., Jr.; Evanseck, J. D.; Field, M. J.; Fischer, S.; Gao, J.; Guo, H.; Ha, S.; et al. All-Atom Empirical Potential for Molecular Modeling and Dynamics Studies of Proteins. *J. Phys. Chem. B* **1998**, *102*, 3586−3616.
(24) MacKerell, A. D.; Feig, M.; Brooks, C. L. Extending the Treatment of Backbone Energetics in Protein Force Fields: Limitations of Gas-Phase Quantum Mechanics in Reproducing Protein Conformational Distributions in Molecular Dynamics Simulations. *J. Comput. Chem.* **2004**, *25*, 1400−1415.
(25) Abraham, M. J.; Murtola, T.; Schulz, R.; Páll, S.; Smith, J. C.; Hess, B.; Lindahl, E. GROMACS: High Performance Molecular Simulations Through Multi-Level Parallelism from Laptops to Supercomputers. *SoftwareX* **2015**, *1*, 19−25.
(26) Patriksson, A.; van der Spoel, D. A Temperature Predictor for Parallel Tempering Simulations. *Phys. Chem. Chem. Phys.* **2008**, *10*, 2073−2077.
(27) Hess, B. Determining the Shear Viscosity of Model Liquids from Molecular Dynamics Simulations. *J. Chem. Phys.* **2002**, *116*, 209−217.
(28) Sorin, E. J.; Pande, V. S. Nanotube Confinement Denatures Protein Helices. *J. Am. Chem. Soc.* **2006**, *128*, 6316−6317.
(29) Ramachandran, G. N.; Ramakrishnan, C.; Sasisekharan, V. Stereochemistry of Polypeptide Chain Configurations. *J. Mol. Biol.* **1963**, *7*, 95−99.
(30) Scholtz, J. M.; Baldwin, R. L. The Mechanism of α-Helix Formation by Peptides. *Annu. Rev. Biophys. Biomol. Struct.* **1992**, *21*, 95−118.
(31) Silbey, R.; Alberty, R.; Bawendi, M. *Physical Chemistry*, 4th ed.; John Wiley & Sons: Hoboken, NJ, 2004.
(32) Makhatadze, G. I. Thermodynamics of α-Helix Formation. *Adv. Protein Chem.* **2005**, *72*, 199−226.
(33) Gnanakaran, S.; García, A. E. Helix-Coil Transition of Alanine Peptides in Water: Force Field Dependence on the Folded and Unfolded Structures. *Proteins: Struct., Funct., Genet.* **2005**, *59*, 773−782.
(34) Dahal, U. R.; Dormidontova, E. E. Spontaneous Insertion, Helix Formation, and Hydration of Polyethylene Oxide in Carbon Nanotubes. *Phys. Rev. Lett.* **2016**, *117*, 027801.

DOI: 10.1021/acs.jpclett.6b02620
J. Phys. Chem. Lett. 2017, 8, 494−499